Journal of Dental Sciences 19 (2024) S26–S37

Available online at www.sciencedirect.com

ScienceDirect

journal homepage: www.e-jds.com

Original Article

Differential expression of osteoblast-like cells on self-organized titanium dioxide nanotubes

Aobo Ma [a], Yiding Zhang [b,c], Junduo Chen [a], Lu Sun [a,d], Guang Hong [a,e*]

[a] *Division for Globalization Initiative, Liaison Center for Innovative Dentistry, Tohoku University Graduate School of Dentistry, Sendai, Japan*
[b] *Department of Periodontology, Shanghai Stomatological Hospital & School of Stomatology, Fudan University, Shanghai, China*
[c] *Shanghai Key Laboratory of Craniomaxillofacial Development and Diseases, Fudan University, Shanghai, China*
[d] *Department of Prosthodontics, College of Stomatology, Dalian Medical University, Dalian, China*
[e] *Department of Prosthodontics, Faculty of Dental Medicine, Universitas Airlangga, Surabaya, Indonesia*

Received 12 July 2024; Final revision received 2 September 2024
Available online 16 September 2024

KEYWORDS
TiO_2 nanotubes;
Dental implant;
Biomaterials;
Cell behavior;
Osteoblast

Abstract *Background/purpose:* Titanium dioxide nanotube (TNT) structures have been shown to enhance the early osseointegration of dental implants. Nevertheless, the optimal nanotube diameter for promoting osteogenesis remains unclear due to variations in cell types and manufacture of nanotubes. This study aimed to evaluate the differences in MC3T3-E1 and Saos-2 cells behavior on nanotubes of varying diameters.
Materials and methods: TNT structures were fabricated by anodizing titanium foil at voltages ranging from 15V to 70V and annealed at 450 °C. Surface morphology and wettability were characterized using field emission scanning electron microscopy and water contact angle measurements, respectively. MC3T3-E1 and Saos-2 cells were cultured to evaluate biocompatibility. Early cell morphology and adhesion were visualized by scanning electron microscopy. Cell proliferation was quantified using CCK-8 assays, and differentiation was assessed through alkaline phosphatase assays. Osteogenesis-related gene expression was analyzed by real-time polymerase chain reaction (PCR), measuring runt-related transcription factor 2 (Runx-2), alkaline phosphatase (ALP), collagen type 1 (COL-1), osteocalcin (OCN), and Osteopontin (OPN) gene levels.
Results: Our results found that Saos-2 cells may be more suitable for TNT-related studies compared to MC3T3-E1 cells. Notably, the 65V nanotube group, with a diameter of 135.9 ± 15.83 nm, demonstrated the most significant osteogenic effect in our assays.

* Corresponding author. Division for Globalization Initiative, Liaison Center for Innovative Dentistry, Tohoku University Graduate School of Dentistry, Sendai, Japan.
E-mail address: hong.guang.d6@tohoku.ac.jp (G. Hong).

https://doi.org/10.1016/j.jds.2024.09.001

Conclusion: We propose that the use and screening of multiple cell lines prior to the evaluation of biomaterials can lead to more accurate in vitro experiments, thereby enhancing the reliability of biomaterial research.

Introduction

Since the introduction of the concept of osseointegration, the development of dental implant materials has traditionally focused on enhancing surface modification and shape processing techniques for hard tissue implant materials.[1,2] Despite the numerous modified materials that demonstrate exceptional physical and chemical properties and commendable biosafety, only a few modified materials (e.g., sandblasted and acid-etched) have successfully transitioned to commercialization for clinical applications. One factor is cost; moreover, the divergence between in vivo and in vitro results can lead to experimental failures, thereby posing a significant barrier to widespread commercialization.[3] In vitro study, biomaterials are typically evaluated by culturing osteoblasts to assess osteocompatibility, hard tissue regeneration, and osteoinductive and osteoconductive properties.[4] Therefore, to reduce the discrepancy between in vitro and in vivo experimental results, it has been suggested that an in vitro model accurately simulating bone formation in vivo should be established before evaluating biomaterials.[5] And the evaluation of cell types should also be considered.

Electrochemical anodizing is a viable method for the surface treatment of dental implants, resulting in titanium dioxide nanotube (TNT) surfaces with antimicrobial potential and osteoinductive properties.[6—8] Existing research has concentrated on exploiting the super hydrophilicity and high surface energy of titanium dioxide nanotubes to enhance cell proliferation, as well as utilizing their unique tubular structure for drug loading and controlled release.[9] While previous studies have demonstrated that variations in TNT tubular diameter influence cell behavior—a notion that has gained wide acceptance—advancements in nanotube fabrication technology have led to the production of nanotubes with more uniform and consistent diameters. This progress facilitates the identification of optimal conditions for the preparation of titanium dioxide nanotubes to promote early osteogenesis.[10,11]

TNT structures with both low and high tubular diameters have been shown to produce favorable cellular outcomes. However, discrepancies in cell usage and preparation methods across studies present challenges for researchers in selecting optimal nanotube preparation and cell culture conditions for subsequent experiments.[12,13] Few studies have concurrently controlled for discrete nanotube diameters, and variations in coating hydrophilicity, and employed different cell lines to validate their findings. In this study, we synthesized nanotubes with varying diameter gradients through precise voltage adjustments and modulated their hydrophilicity via annealing. We then evaluated the effects of these nanotube structures on the proliferation and osteogenesis of the well-characterized MC3T3-E1 and Saos-2 cell lines. The primary aim was to elucidate the influence of titanium dioxide nanotube size on osteoblast-like cells. Furthermore, we propose that in vitro models of dental hard tissue biomaterials should utilize a variety of cell lines to achieve more accurate predictions in vivo outcomes.

Materials and methods

Fabrication of titanium dioxide nanotube structures

As a substrate for TNT growth, we used 1 cm × 1cm, square shape titanium foil with a thickness of 0.1 mm (99.6% purity), which was degreased by ultrasonication in 75% acetone and methanol, then rinsed with deionized water (DI) and dried in a desiccator. The electrolyte utilized for gradient TiO_2 nanotube arrays comprised 0.16 mol/L NH_4F (FUJIFILM Wako Pure Chemical Corporation, Osaka, Japan), 10 vol% H_2O, and ethylene glycol (EG, FUJIFILM Wako Pure Chemical Corporation). The titanium foil was used as the working electrode, and the platinum plate was used as the counter electrode with a working distance of 25 mm. The reaction was carried out at 20 °C for 1 h at different voltages (15V—70V with 5V intervals) and stored in EG for 24h. All samples were ultrasonically cleaned in deionized water for 2 min, dried naturally, annealed at 450 °C for 1 h, and sterilized by autoclaving.

Surface morphology and wettability

The wetting properties of the sample surface were assessed by measuring its static water contact angle. A microsyringe (PCA-1, KYOWA, Saitama, Japan) carefully deposited a distilled water droplet (4 μl) onto the sample surface. The contact angle was determined by numerically fitting the droplet images and estimated with an error of ±1°. To obtain more accurate images, the morphology of the nanotubes was characterized with a field emission scanning electron microscope (FESEM, Hitachi SU5000, Tokyo, Japan). Pore sizes were measured using the ImageJ software.

Cell culture

Murine MC3T3-E1 subclone 14 osteoprogenitor cells (CRL-2594, ATCC, Rockville, MD, USA) and Human osteoblast-like Saos-2 cells (85-HTB, ATCC) are commonly used osteoblast cell lines, and frozen cells up to three generations old were used for cellular experiments. Alfa-minimum essential

medium (Nacalai Tesque, Kyoto, Japan) was used to cultivate the MC3T3-E1 cells, and 1640 medium (Nacalai Tesque) was used to cultivate Saos-2, supplemented with 10 % fetal bovine serum (FBS), 1% Glutamine (Nacalai Tesque), and penicillin/gentamycin (Nacalai Tesque) at 37 °C with 5 % CO_2. A 60 mm cell culture dish was used as the culture vessel, and cells were cultured at a density of 10,000 cells/cm^2 to confluence and applied to subsequent experiments.

Cell morphology

To examine cell morphology on various surfaces, 10,000 cells/cm^2 of MC3T3-E1 and Saos-2 were seeded on different samples in 24 wells and incubated for 12 and 24 h, respectively. At the end of the incubation period, all samples were rinsed twice with PBS and then fixed at 4 °C in 2.5% glutaraldehyde solution overnight. The fixed cells were then rinsed three times with PBS for 10 min each and sequentially dehydrated with ethanol solutions (60%, 70%, 80%, 90%, 95%, and 100% v/v). The samples were then placed in fresh t-butyl alcohol (FUJIFILM Wako Pure Chemical Corporation) for 20 min, a process repeated three times. Following this, the samples were placed in metal containers, with 50 μl of t-butyl alcohol added to the surface, and frozen at −20 °C for 2 h. After freezing, the containers were placed in a freeze-drying device (JFD-320, JEOL, Tokyo, Japan), where the residual water in the samples was displaced by t-butyl alcohol and dried by sublimation of t-butyl alcohol under freezing conditions, preserving cell morphology. To enhance the electrical conductivity of the samples, a platinum coating was applied using an auto-fine coater (JFC-1600, JEOL, Tokyo, Japan). Finally, cells grown on the various samples were observed using a Scanning Electron Microscope (JSM-6390LA, JEOL, Tokyo, Japan).

Cell proliferation

Cells were seeded on the surface of different samples using the same procedures as in the previous experiment. The cells were incubated in cell chambers for 1, 4, and 7 days, and cell activity was measured using a cell counting kit (CCK-8, Dojindo, Kumamoto, Japan). After each observation time, the conditioned medium was replaced with 30 μL of CCK-8 reagent, and 330 μL of culture medium was diluted per well and incubated for an additional 1 h. Absorbance was measured at 450 nm using a Bio-Rad iMark Microplate Absorbance Reader (Bio-Rad, Hercules, CA, USA).

Cell differentiation

An alkaline phosphatase kit assessed the early stage of cell differentiation. Cells were seeded and cultured using the previously described method for 14 days, with medium changes every two days. After 14 days, cells in plates were washed three times with PBS and incubated with 1% (v/v) Triton X-100 at 37 °C for 15 min to lyse the cells. The reaction was terminated with 0.1 M NaOH after 30 min at 37 °C using ALP reaction solution combined with supernatant according to the manufacturer's instructions, and the absorbance was measured at 415 nm. Total cellular protein concentration was determined using a bicinchoninic acid (BCA) protein assay kit (Takara Bio, Shiga, Japan), measuring absorbance at 595 nm.

Osteogenesis-related gene expression

To detect the expression levels of osteoblast-related genes in different groups of cells, cells were cultured for 14 days and then assayed using the real-time PCR method. Total RNA from each group was isolated using RNAiso Plus reagent (Takara Bio) and reverse transcribed to cDNA using the iScript Advanced cDNA Synthesis kit (Bio-Rad, Hercules, CA, USA). PCR was extracted on a CFX96 Real-time PCR analysis was performed on a CFX96 Touch Deep Well real-time PCR system (Bio-Rad) using SsoAdvanced™ Universal SYBR® Green Supermix (Bio-Rad). Primers used in this study were Runx2, ALP, COL-1, OCN, and OPN, with the housekeeping gene Glyceraldehyde-3-phosphate dehydrogenase (GAPDH) used as the internal control. The results were calculated using the $2^{-\Delta\Delta Ct}$ method to calculate the data. The primers used for the target and housekeeping genes are listed in Tables 1 and 2.

Table 1 Primers for mouse osteogenesis-related genes.

Gene	Genebank ID	DNA Primer	Sequence	Size (bp)
Mus Runx-2	NM_009820.6	FORWARD	5′- CCCAGCCACCTTTACCTACA -3′	150
		REVERSE	5′- TATGGAGTGCTGCTGGTCTG -3′	
Mus ALP	NM_007431.3	FORWARD	5′-ATCTTTGGTCTGGCTCCCATG-3′	106
		REVERSE	5′-TTTCCCGTTCACCGTCCAC-3′	
Mus COL1	NM_007742.4	FORWARD	5′-TAAGGGTCCCCAATGGTGAGA-3′	203
		REVERSE	5′-GGGTCCCTCGACTCCTACAT-3′	
Mus OCN	NM_007541.3	FORWARD	5′-GGACCATCTTTCTGCTCACTCTG-3′	131
		REVERSE	5′-GTTCACTACCTTATTGCCCTCCTG-3′	
Mus OPN	NM_001204203.1	FORWARD	5′-CTCACATGAAGAGCGGTGAG-3′	174
		REVERSE	5′-TCTCCTGGCTCTCTTTGGAA-3′	
Mus GAPDH	NM_008084.3	FORWARD	5′-GGTGAAGGTCGGTGTGAACG-3′	233
		REVERSE	5′-CTCGCTCCTGGAAGATGGTG-3′	

Abbreviations: runt-related transcription factor 2, Runx-2; alkaline phosphatase, ALP; collagen type 1, COL-1; osteocalcin, OCN; osteopontin, OPN.

Table 2 Primers for human osteogenesis-related genes.

Gene	Genebank ID	DNA Primer	Sequence	Size (bp)
Homo Runx-2	NM_001024630.4	FORWARD	5′-GGTTAATCTCCGCAGGTCACT-3′	143
		REVERSE	5′-CACTGTGCTGAAGAGGCTGTT-3′	
Homo ALP	NM_001632.5	FORWARD	5′-GACAAACTGGGGCCTGAGATA-3′	247
		REVERSE	5′-CTGACTTCCCTGCTTTCTTGG-3′	
Homo COL1	NM_000089.4	FORWARD	5′-ACAAGGCATTCGTGGCGATAAGG-3′	106
		REVERSE	5′-ACCAGCGATACCAGGCAGACC-3′	
Homo OCN	NM_199173.6	FORWARD	5′-TCACACTCCTCGCCCTATTG-3′	242
		REVERSE	5′-AGCCAACTCGTCACAGTCC-3′	
Homo OPN	NM_000582.3	FORWARD	5′-ACTGATTTTCCCACGGACCT-3′	192
		REVERSE	5′-CTCCTCGCTTTCCATGTGTG-3′	
Homo GAPDH	NM_002046.7	FORWARD	5′-TCAAGAAGGTGGTGAAGCAGG-3′	115
		REVERSE	5′-TCAAAGGTGGAGGAGTGGGT-3′	

Abbreviations: runt-related transcription factor 2, Runx-2; alkaline phosphatase, ALP; collagen type 1, COL-1; osteocalcin, OCN; osteopontin, OPN.

Statistical analysis

All experiments were repeated three times, and the data were expressed as mean ± standard deviation (SD). One-way analysis of variance (ANOVA) and Tukey's post hoc test were used to test for statistical differences between samples. All differences were significant when $P < 0.05$. For the results of this experiment, the considerable difference in the letter labeling method indicates the means of different groups by different letters (e.g., "a," "b," "c"). Means with the same letter are not significantly different, while means with different letters are significantly different.

Results

Nano surface characterization

Anodic oxidation experiments produced TNT structures on the surface of titanium foil (Fig. 1). The narrow size distribution of the nanotube inner diameters indicates excellent homogeneity and the surface finish of the TNT coating at different voltages (Fig. 2A). Visible cracks appeared on the nanotube coating at voltages between 30V and 55V. In contrast, fewer cracked structures were observed at anodic oxidation voltages ranging from 15V to 25V and 60V to 70V (Fig. 2A). Histograms of nanotube diameters along with their respective Gaussian fits for each experimental condition (Fig. 2B). The measured diameters were as follows: 41.8 ± 5.4 nm at 15V, 43.1 ± 6.6 nm at 20V, 49.6 ± 7.7 nm at 25V, 60.6 ± 7.7 nm at 30V, 75.9 ± 10.5 nm at 35V, 84.3 ± 13 nm at 40V, 94.2 ± 11.4 nm at 45V, 102.6 ± 12.1 nm at 50V, 88.7 ± 24.9 nm at 55V, 110.7 ± 8.5 nm at 60V, 135.9 ± 15.8 nm at 65V, and 115.9 ± 17.1 nm at 70V (Fig. 2C).

The water contact angle on the surface of the nanotube structure is significantly lower than that on pure titanium (Fig. 3A). The contact angles for each group are as follows: 88.2 ± 0.4° for pure titanium, 10.5 ± 0.6° for 15V, 13.7 ± 1.7° for 20V, 11.6 ± 1.8° for 25V, 11.3 ± 0.6° for 30V, 6.1 ± 0.3° for 35V, 6.5 ± 0.8° for 40V, 4.4 ± 0.4° for 45V, 6.5 ± 0.4° for 50V, 5.1 ± 1.1° for 55V, 5.2 ± 0.7° for 60V, 4.1 ± 0.4° for 65V, 5.4 ± 0.6° for 70V (Fig. 3B).

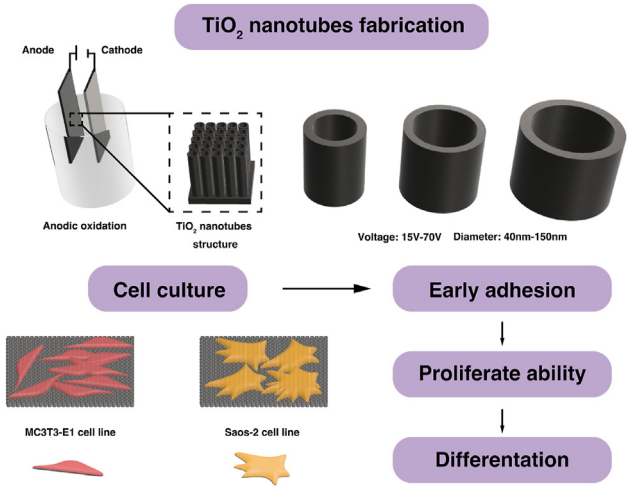

Figure 1 Schematic diagram illustrating the preparation of titanium dioxide nanotubes (TNT) and the associated cellular experiments.

Osteoblast-like cell behaviors on nanotube

MC3T3-E1 cells were incubated on the sample surface for 12 and 24 h, and early cell adhesion patterns were observed using SEM (Fig. 4). The results demonstrated that the cells exhibited a typical fibroblast-like shape. Notably, there was a distinct difference in cell morphology between the nanotube and pure titanium groups.

Saos-2 cells were also incubated on the sample surface for 12 and 24 h to observe different cell morphologies (Fig. 5). The cell morphology is typical of an irregular epithelioid cell pattern, and there were also large differences in cell morphology between the different nanotube groups. At the same time, the cells became more malleable and had a larger surface area as the inoculation time increased.

While there was a variance in the cell proliferation ability of MC3T3-E1 on various material surfaces, the

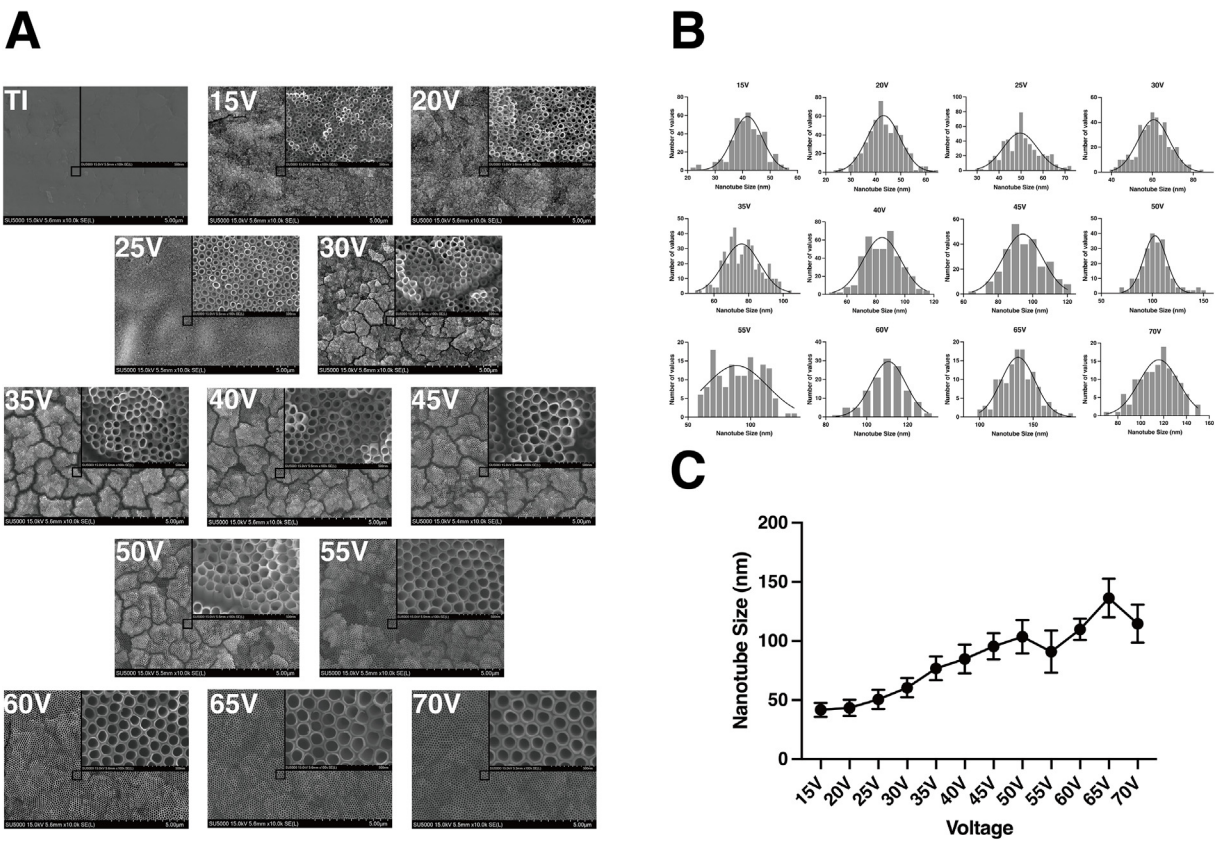

Figure 2 The results of nanotube surface characterization. (A) Surface micromorphology images of different substrates were obtained with scanning electron microscope, respectively (10,000 ×, scale bar = 5 μm). Insets of images were magnified scanning electron microscope graphs (100,000 ×, scale bar = 500 nm). (B) Histograms of the diameter of titanium dioxide nanotubes in different groups with fitted curves. (C) Line graph showing the growth trend of titanium dioxide nanotubes.

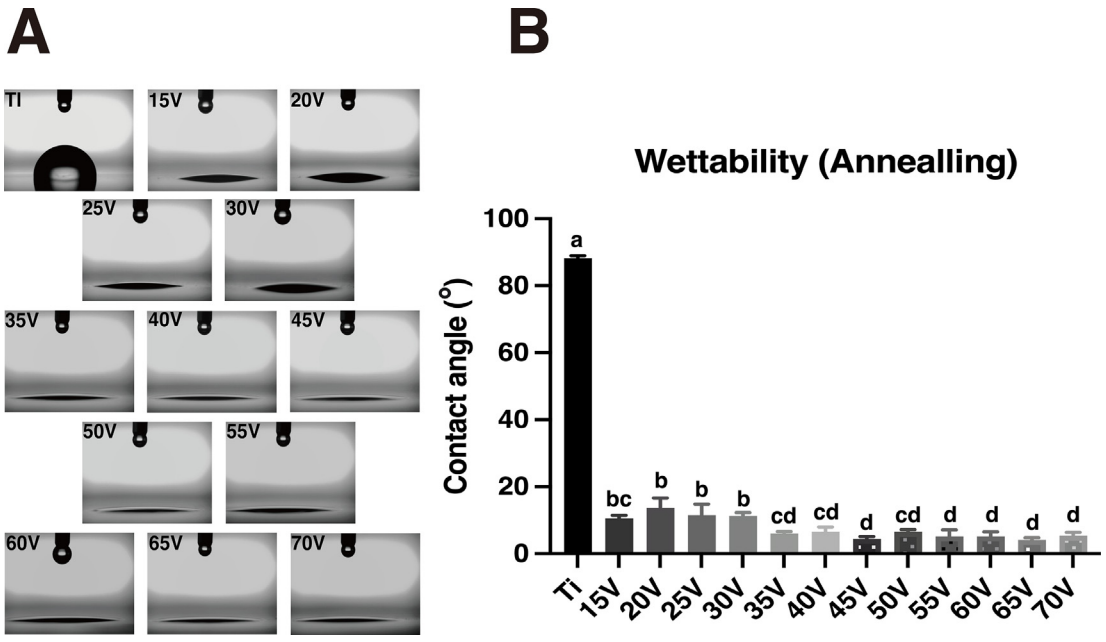

Figure 3 Contact angles of various samples. (A) Images of contact angles on different surfaces; (B) Contact angle values of different surfaces. Data are expressed as mean ± SD, n = 3 replicates per group. Different lowercase letters indicate statistically significant differences between groups ($P < 0.05$). Data are presented as mean ± SD, with n = 3 replicates for each group.

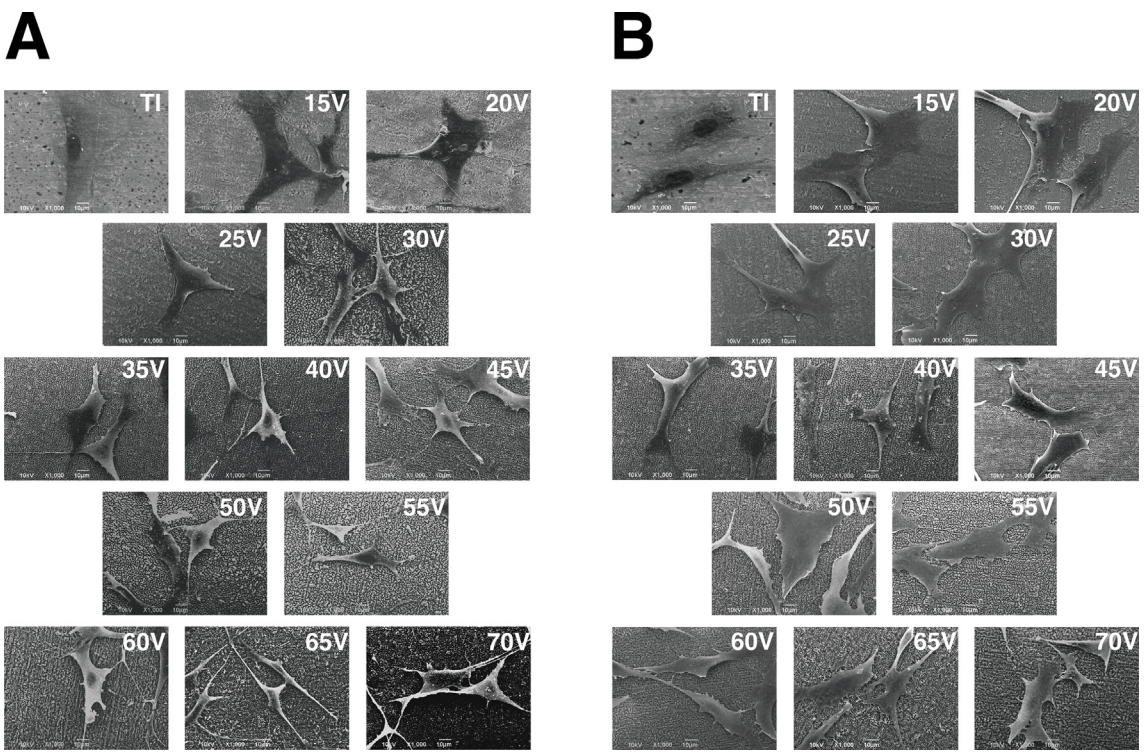

Figure 4 Morphological images of MC3T3-E1 cells were obtained by scanning electron microscopy. (A) MC3T3-E1 cells were cultured on different substrates for 12 h; (B) MC3T3-E1 cells were cultured on different substrates for 24 h (1000 $\times$, scale bar $=$ 10 μm).

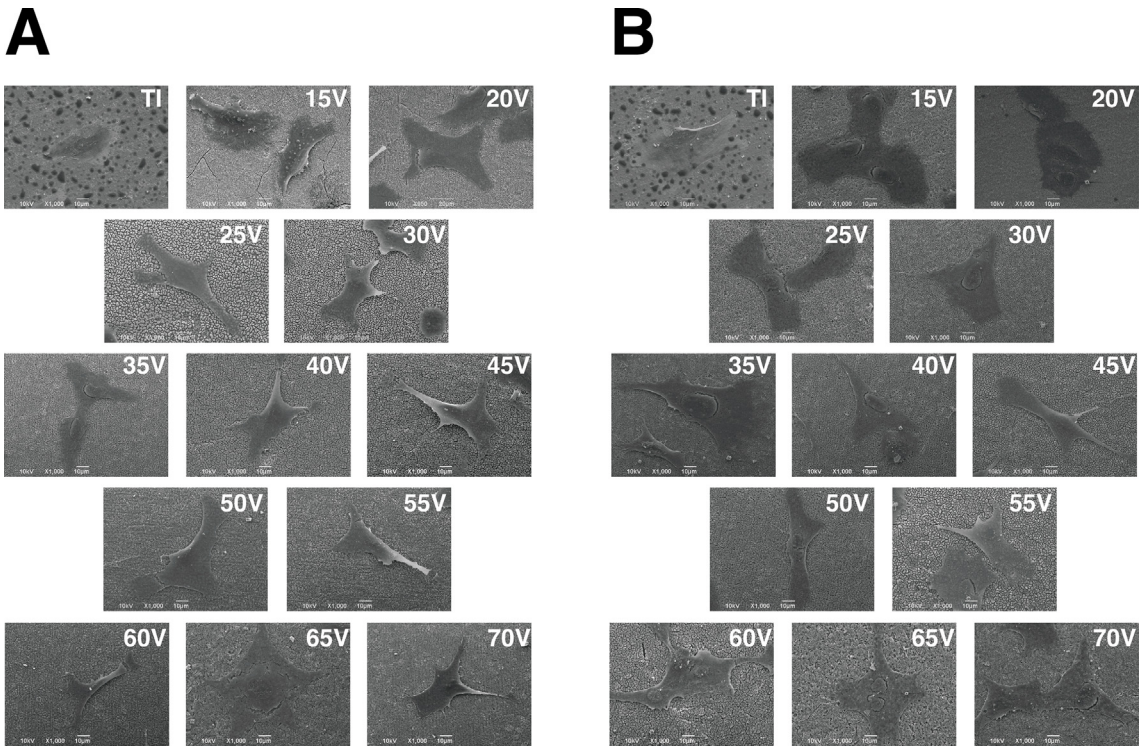

Figure 5 Morphological images of Saos-2 cells were obtained by scanning electron microscopy. (A) Saos-2 cells were cultured on different substrates for 12 h; (B) Saos-2 cells were cultured on different substrates for 24 h (1000 $\times$, scale bar $=$ 10 μm).

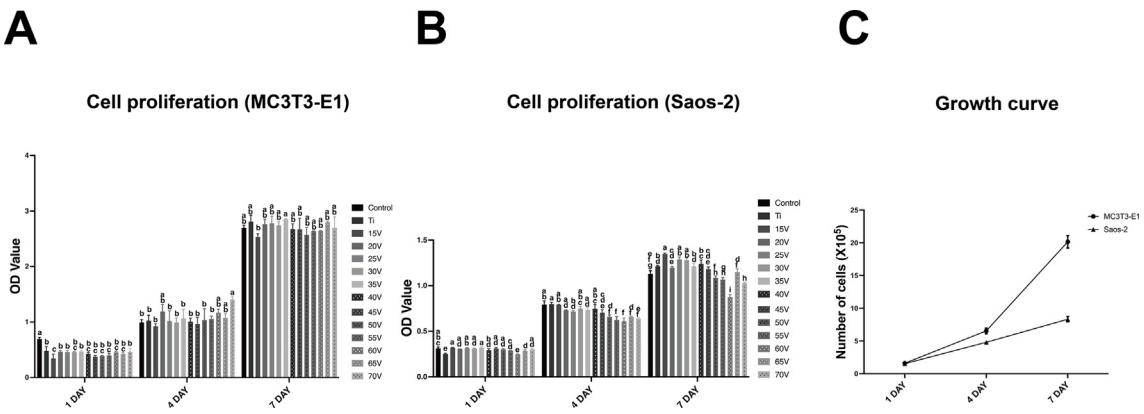

Figure 6 Cell proliferation results of different samples. (A) MC3T3-E1 cells were cultured on different surfaces for 1, 4, and 7 days; (B) Saos-2 cells were cultured on different surfaces for 1, 4, and 7 days. Different lowercase letters indicate statistically significant differences between groups ($P < 0.05$). Data are presented as mean ± SD, with n = 3 replicates for each group.

observed differences were predominantly not statistically significant overall (Fig. 6A). But significant differences in cell proliferation were evident in Saos-2 cells (Fig. 6B). And proliferation rate of MC3T3-E1 cells was higher than Saos-2 cells (Fig. 6C).

Differentiation and gene expression

After 14 days of culture, both cell types exhibited comparable differentiation trends across various sample surfaces (Fig. 7). Except for the comparison between the 65V and 70V groups, there were no significant differences observed in MC3T3-E1 cells across the various nanotube groups (Fig. 7A). The differentiation ability of Saos-2 cells was essentially enhanced with increasing nanotube diameter, reaching its peak in the 65V group (Fig. 7B).

Saos-2 cells demonstrated a more homogeneous osteogenic gene expression profile, with significantly elevated levels of ALP, COL-1, OCN, and OPN in the high-tubular diameter group, particularly at 65V, compared to pure titanium (Fig. 8B). Conversely, the MC3T3-E1 group exhibited an unstable expression pattern, with elevated levels of osteogenesis-related genes at 30V, 50V, and 60V (Fig. 8A). Moreover, MC3T3-E1 cells did not exhibit an enhanced osteogenic differentiation trend when exposed to nanotube structures relative to pure titanium.

Discussion

Compared to previous experiments, the TNT structure was successfully obtained with a shorter reaction time of 1 h.[14] In this experiment, the third-generation TNT anodizing technique was employed, which produces relatively ordered nanotube structures compared to the first and second generations, thereby excluding the effect of diameter variations within the group.[15] Recent studies indicate that

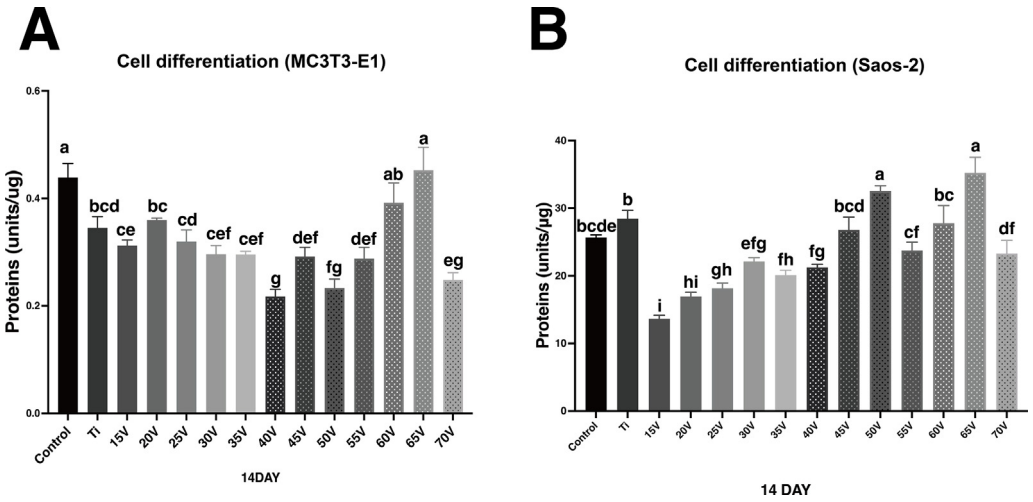

Figure 7 Cell differentiation results of different samples. (A) MC3T3-E1 cells were cultured on different surfaces for 14 days; (B) Saos-2 cells were cultured on different surfaces for 14 days. Different lowercase letters indicate statistically significant differences between groups ($P < 0.05$). Data are presented as mean ± SD, with n = 3 replicates for each group.

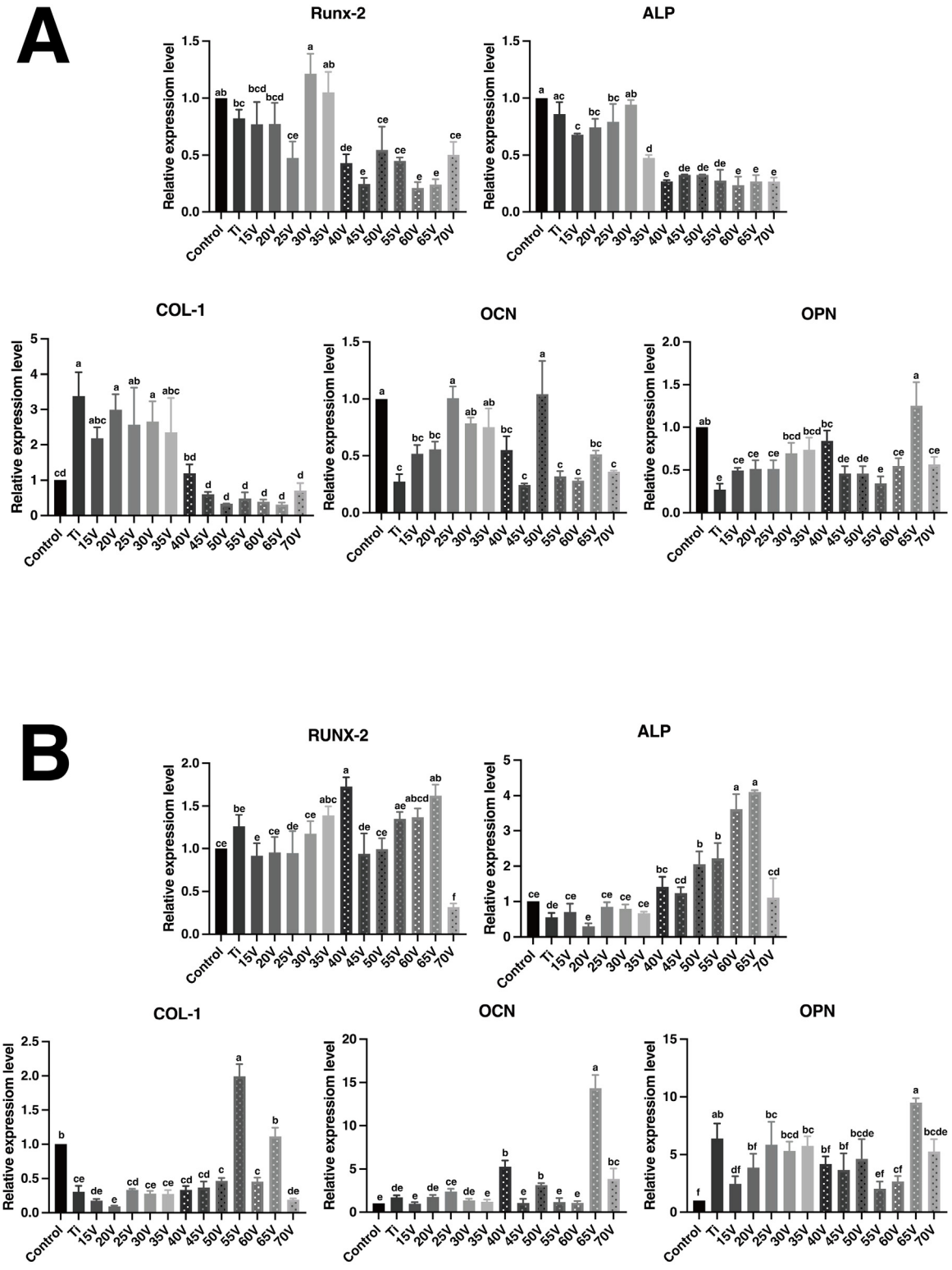

Figure 8 Real-time PCR results of runt-related transcription factor 2 (Runx-2), alkaline phosphatase (ALP), collagen type 1 (COL-1), osteocalcin (OCN), and osteopontin (OPN) gene expression levels in MC3T3-E1 cells (A) and Saos-2 cells (B) after 14 days of culture on different samples. Different lowercase letters indicate statistically significant differences between groups ($P < 0.05$). Data are presented as mean ± SD, with n = 3 replicates per group.

the growth rate of crack density in anodizing processes follows a power-law relationship with the anodizing voltage, where the power exponent decreases with increasing anodizing temperature.[16] In the current experiment, a rise in electrolyte temperature was observed with increasing voltage during the anodizing reaction, which attributed to Joule heating caused by the current, exothermic reactions at the electrodes, and resistive heating within the electrolyte.[17] Due to the limitations of the cooling system and the ambient temperature, along with the gradual warming of the electrolyte in the 30V—50V voltage range, precise monitoring and control of the electrolyte temperature were challenging. Consequently, visible cracks were detected in the imaging results for these experimental groups.

By comparing the tube sizes, the 55V group exhibits significant variability in nanotube diameters compared to other groups, deviating from a normal distribution and lacking a well-fitted Gaussian curve. Concurrently, the mean diameter values at 55V and 70V do not follow a linear correlation in the plotted line graph. This discrepancy could be attributed to fluctuations in electrolyte temperature and ambient temperature. However, the variation in experimental conditions does not undermine the overall conclusion: higher voltage leads to increase in nanotube diameters and a broader distribution of those diameters.

According to previous studies, the TNT structure provides a permeable space for liquid, reducing the contact angle and making the surface more hydrophilic. TNT demonstrates high surface energy at elevated voltages, and the TNT structure allows for greater permeation space as the tube diameter increases.[18,19] Upon annealing, the TNT surface becomes superhydrophilic due to the formation of anatase.[20] In this experiment, starting with the 35 V group (diameter of 75.9 $\pm$ 10.5 nm), the contact angle remains constant despite variations in TNT diameter.

Early cell adhesion is a critical process where cells attach to the extracellular matrix (ECM) or other cells. This process begins with the recognition and binding of specific molecules on the cell surface to ligands in the ECM or on adjacent cells.[21] Previous studies have shown that the significantly smaller surface area of the flattened titanium substrate with fewer topological cues compared to the TNT group may not be sufficient for optimal cell attachment.[22] After 12 and 24 h of incubation, MC3T3-E1 cells on the surface of the nanotubes showed more pronounced filopodia with significantly longer structures and a higher degree of contact compared to pure titanium (Fig. 4). This behavior is consistent with previous osteoblast observations, where the interaction between cells and nanotubes enhanced cell dissemination and overall cell—substrate interaction.[23,24] However, the changes in MC3T3-E1 cell morphology across different groups of nanotubes over various time points are relatively small. In contrast, Saos-2 cells exhibited morphological differences on TNT surfaces with varying tube sizes. After 12 h of incubation, cells in all TNT groups displayed filopodia structures and typical epithelial cell morphology compared to smooth pure titanium. However, after 24 h of incubation, the cell area in the TNT group at voltages lower than 35V enlarged, and colonies formed between the cells. At voltages exceeding 35V, although the cell morphology still showed extended filopodia and maintained a tendency for contact, there was still a tendency for the cells to form colonies. This phenomenon is related to differences in material hydrophilicity and may be influenced by the stronger hydrophilicity of the TNT structure above 35V. Similarly, a previous study showed that nanotube structures with a tube diameter larger than 75 nm are beneficial for cell adhesion, which is consistent with the results of this experiment.[25]

To evaluate the biocompatibility of anodized surfaces, we studied the cell viability of different osteoblast-like cell types. The proliferation efficiency of MC3T3-E1 cells was significantly higher than that of Saos-2 cells within 7 days. This is likely due to MC3T3-E1 cells forming multilayered cell stacks under specific culture conditions, resulting in vertical growth, a phenomenon not observed with Saos-2 cells.[26] In the differential cellular presence on the nanotube surface is not evident due to the high proliferative activity of MC3T3 cells. In contrast, Saos-2 cells exhibited notable variability on different nanotube surfaces on the fourth and seventh days. While previous studies have demonstrated the impact of nanotube structures on cellular behavior, it is essential to consider the inherent proliferative tendencies of cells when comparing different nanotube structures.[27] The excessive proliferation of cells may influence the efficacy of various nanotube structures in promoting cell proliferation. Given the low proliferative capacity of human osteoblasts compared to cell lines, selecting a cell line with a lower proliferative capacity for biomaterials experiments may yield more rigorous results.[28] The proliferation rate of MC3T3-E1 cells was significantly higher than that of Saos-2 cells and similar with the previous study.[29] At the same time, there is basically no significant differences observed among the different experimental groups for MC3T3-E1 cells. Consequently, in this study, analyzing the proliferation ability of Saos-2 cells may provide more meaningful insights than those of MC3T3-E1 cells. On the first day, cell numbers increased in all nanotube groups compared to pure titanium, except for the 60V group. This observed trend may be attributed to the superhydrophilicity of the nanotube structure, which facilitates early cell adhesion and consequently enhances the initial cell proliferation capacity.[10] However, on the fourth day, cell proliferation diminished as the nanotube diameter increased. This trend persisted into the seventh day, with cell proliferative capacity mirroring a similar pattern as on the fourth day. Notably, the 15V nanotube group exhibited a significantly higher pro-proliferative capacity compared to pure titanium on both the fourth and seventh days, suggesting a strong influence of nanotube diameter on cell proliferation. This finding aligns with previous studies indicating that low-diameter nanotubes promote cell proliferation. Conversely, the high-diameter nanotube groups after 50V significantly decreased cell proliferation compared to pure titanium and control groups especially in the 60 V group. This observation suggests that nanotubes with a larger diameter promote cell differentiation while inhibiting cell proliferation, consistent with previous findings.[30,31]

Alkaline phosphatase (ALP) is abundantly expressed in mineralized tissue cells and plays a critical role in the biomineralization process essential for hard tissue formation.[32] Relative to the control and pure titanium groups,

samples with larger nanotube diameters, particularly the 65V group, exhibited significantly enhanced cellular differentiation. The differentiation trend of Saos-2 cells positively correlated with nanotube diameter, peaking in the 65V nanotube group (135.9 ± 15.83 nm). This trend is consistent with the previous distribution of nanotube diameters (Fig. 2). The differentiation trend of MC3T3-E1 cells was less pronounced than Saos-2 and showed an opposite trend at 50V. Previous studies have shown that the basal alkaline phosphatase activity of Saos-2 cells is 100 to 1000 times higher than that of other established human osteogenic sarcoma cell lines. In the present experiments, the alkaline phosphatase activity of Saos-2 cells was nearly 100-fold higher than that of the corresponding MC3T3-E1 cells in all groups.[33] We hypothesize that the low expression of ALP in MC3T3-E1 cells mitigates the influence of the TNT structure on cellular osteogenic differentiation, thereby reducing the variability in the effects of different TNT structures. Additionally, the absence of osteogenic inducers in the MC3T3-E1 cell culture and the limited 14-day culture period, as opposed to the 21 days, likely prevented the nanotube structure's full impact on MC3T3-E1 cell differentiation from being observed. However, this result provides side evidence that Saos-2 cells can achieve promising differentiation outcomes within a shorter timeframe when evaluating TNT materials for cellular pro-differentiation. The superior properties of this cell line may also render it suitable for studies involving other biomaterials.

In addition to alkaline phosphatase (ALP) assays, evaluating the expression of osteogenic genes is essential for a comprehensive assessment of osteoblast differentiation and functionality. The expression and activity of Runx-2 and ALP are pivotal markers of early osteogenic differentiation, with Runx2 gene upregulation typically accompanied by increased expression of COL-1, OCN, and OPN.[34,35] There was no clear trend in the expression of osteogenesis-related genes in the MC3T3-E1 cell model, with high expression occurring in both the high and low nanotube diameter groups. Additionally, the nanotube groups did not show better osteogenic gene expression than the control and pure titanium groups. But similar to the results of the ALP experiments, Saos-2 cells exhibited more pronounced trends compared to MC3T3-E1 cells. This was particularly evident in the ALP gene assay, where the expression of ALP genes increased with increasing nanotube diameter, peaking at 65V. COL-1, OCN, and OPN gene expression also peaked at 65V, providing a crucial indication for our group's focus in subsequent experiments. This also suggests that Saos-2 cells may be more suitable for nanotube research experiments than the MC3T3-E1 cell model.

As a result of the anodizing experiments, high voltage induces a thermal effect according to Joule's law. To maintain a constant voltage, the current gradually increases, leading to a further rise in the temperature of the reaction solution. Consequently, instability in temperature regulation may affect the experimental outcomes. In this experiment, the reaction at 70 V generated excessive heat, and the cooling equipment was unable to maintain the stability of the reaction solution temperature. Therefore, SEM analysis revealed that while the average tube diameter at 70 V is similar to that at 60 V, the variance is significantly larger.

In osteogenesis experiments, the ALP experiment showed that the 60V and 70V groups exhibited lower differentiation capacity compared to the 65V group. In gene experiments, there was no statistically significant difference in osteogenic gene expression between MC3T3 cells in the 65V and 70V groups. In contrast, in Saos-2 cells, although the difference in osteogenic gene expression between the 65V and 70V groups is more pronounced, it is evident that 60V shows higher expression of early osteogenic genes, such as RUNX-2, ALP, and Col-1, while the late osteogenic genes, OCN and OPN, are more highly expressed at 70V. This suggests that 60V has a strong osteogenic potential; however, this does not necessarily imply that the osteogenic effect of 60V is superior to that of 70V. However, 65V shows a tendency for high expression in both early and late osteogenic genes, a phenomenon that will be investigated in future experiments.

Research on titanium dioxide nanotubes in biological contexts is not a novel topic. As early as 2007, Jung Park et al. demonstrated that nanotube structures with diameters of 15–30 nm significantly accelerated integrin clustering and focal contact formation in rat MSCs, leading to a marked increase in cellular activity.[10] Further studies in 2009 reinforced these findings, showing that nanotubes with diameters of 15–30 nm promote the differentiation of rat MSCs into endothelial and muscle cells more effectively than those with diameters of 100 nm.[12] However, in the same year, an opposing view was presented, suggesting that 100 nm nanotubes could promote osteoblast differentiation more effectively than 15–30 nm nanotubes.[36] Meanwhile, a great deal of research re-examines the question.[37–39] Consequently, the optimal tube size of titanium dioxide nanotubes has remained a subject of debate.

However, most of these studies are based on first- and second-generation nanotube technologies, which often exhibit limitations in terms of nanotube self-assembly ordering and surface smoothness.[15,40] In addition, this experiment improves upon previous studies by increasing the voltage intervals and precisely differentiating between voltage levels. Moreover, it is the first to compare the effects of nanotube structures across different cell lines.

In conclusion, this study suggests that Saos-2 cells would be more suitable for TNT-related studies. The observed differences between MC3T3-E1 and Saos-2 cells highlight that even the same material may yield different results depending on the cell line used for evaluating biomaterials. Additionally, a comparison of samples with different tubular diameters revealed that the 65V (135.9 ± 15.83 nm) group showed the best osteogenic results in the osteogenic assay. The size of these nanotubes will be studied in greater depth in subsequent experiments. Our study provides limited insights into the direct effects of these two cell lines on titanium dioxide nanotubes. Therefore, further studies are needed to establish in vitro experimental conditions that reflect bone formation and regeneration in vivo and to evaluate titanium dioxide nanotubes for more effective and accurate application in dental implants. Nonetheless, this work offers new ideas, suggesting that the use and screening of multiple cell lines allow for more accurate in vitro experiments with biomaterials and offer valuable insights for future research and applications of Tio2 nanotubes.

Declaration of competing interest

The authors have no conflicts of interest relevant to this article.

Acknowledgments

This study was supported by the JST SPRING, Japan (grant number: JPMJSP2114).

References

1. Guglielmotti MB, Olmedo DG, Cabrini RL. Research on implants and osseointegration. *Periodontol* 2000 2019;79:178—89.
2. Duraccio D, Mussano F, Faga MG. Biomaterials for dental implants: current and future trends. *J Mater Sci* 2015;50:4779—812.
3. Kohli N, Ho S, Brown SJ, et al. Bone remodelling in vitro: where are we headed?: -A review on the current understanding of physiological bone remodelling and inflammation and the strategies for testing biomaterials in vitro. *Bone* 2018;110:38—46.
4. Klein SG, Alsolami SM, Arossa S, et al. In situ monitoring reveals cellular environmental instabilities in human pluripotent stem cell culture. *Commun Biol* 2022;5:119.
5. Izumiya M, Haniu M, Ueda K, et al. Evaluation of MC3T3-E1 cell osteogenesis in different cell culture media. *Int J Mol Sci* 2021;22:7752.
6. Kunrath MF, Farina G, Sturmer LBS, et al. TiO2 nanotubes as an antibacterial nanotextured surface for dental implants: systematic review and meta-analysis. *Dent Mater* 2024;40:907—20.
7. Kumaravel V, Nair KM, Mathew S, et al. Antimicrobial TiO2 nanocomposite coatings for surfaces, dental and orthopaedic implants. *Chem Eng J* 2021;416:129071.
8. Pires LA, de Azevedo Silva LJ, Ferrairo BM, et al. Effects of ZnO/TiO2 nanoparticle and TiO2 nanotube additions to dense polycrystalline hydroxyapatite bioceramic from bovine bones. *Dent Mater* 2020;36:e38—46.
9. Jafari S, Mahyad B, Hashemzadeh H, et al. Biomedical applications of TiO2 nanostructures: recent advances. *Int J Nanomed* 2020;15:3447—70.
10. Park J, Bauer S, von der Mark K, et al. Nanosize and Vitality: TiO2 nanotube diameter directs cell fate. *Nano Lett* 2007;7:1686—91.
11. Prakasam HE, Shankar K, Paulose M, et al. A new benchmark for TiO2 nanotube array growth by anodization. *J Phys Chem C* 2007;111:7235—41.
12. Park J, Bauer S, Schmuki P, et al. Narrow window in nanoscale dependent activation of endothelial cell growth and differentiation on TiO2 nanotube surfaces. *Nano Lett* 2009;9:3157—64.
13. Roguska A, Pisarek M, Belcarz A, et al. Improvement of the biofunctional properties of TiO2 nanotubes. *Appl Surf Sci* 2016;388:775—85.
14. Ma A, You Y, Chen B, et al. Icariin/aspirin composite coating on TiO2 nanotubes surface induce immunomodulatory effect of macrophage and improve osteoblast activity. *Coatings* 2020;10:427.
15. Regonini D, Bowen CR, Jaroenworaluck A, et al. A review of growth mechanism, structure and crystallinity of anodized TiO2 nanotubes. *Mater Sci Eng R Rep* 2013;74:377—406.
16. Zhang W, Kang K, Wei A, et al. Anodizing-induced cracking in the preparation of TiO2 nanotube arrays. *Micro Nanostructures* 2023;181:207626.
17. Chiu RL, Chang PH, Tung CH. The effect of anodizing temperature on anodic oxide formed on pure Al thin films. *Thin Solid Films* 1995;260:47—53.
18. Wang D, Liu Y, Liu X, Zhou F, Liu W, Xue Q. Towards a tunable and switchable water adhesion on a TiO2 nanotube film with patterned wettability. *Chem Commun* 2009;45:7018—20.
19. Liu G, Du K, Wang K. Surface wettability of TiO2 nanotube arrays prepared by electrochemical anodization. *Appl Surf Sci* 2016;388:313—20.
20. Shin DH, Shokuhfar T, Choi CK, Lee SH, Friedrich C. Wettability changes of TiO2 nanotube surfaces. *Nanotechnology* 2011;22:315704.
21. Kanchanawong P, Calderwood DA. Organization, dynamics and mechanoregulation of integrin-mediated cell-ECM adhesions. *Nat Rev Mol Cell Biol* 2023;24:142—61.
22. Hao J, Zhang Y, Jing D, et al. Mechanobiology of mesenchymal stem cells: perspective into mechanical induction of MSC fate. *Acta Biomater* 2015;20:1—9.
23. Brammer KS, Oh S, Gallagher JO, Jin S. Enhanced cellular mobility guided by TiO2 nanotube surfaces. *Nano Lett* 2008;8:786—93.
24. Chen CY, Kim DM, Lee C, et al. Biological efficacy of perpendicular type-I collagen protruded from TiO2-nanotubes. *Int J Oral Sci* 2020;12:36.
25. Mansoorianfar M, Tavoosi M, Mozafarinia R, et al. Preparation and characterization of TiO2 nanotube arrays on Ti6Al4V surface for enhancement of cell treatment. *Surf Coat Technol* 2017;321:409—15.
26. Tevlek A, Odabas S, Çelik E, Aydin HM. Preparation of MC3T3-E1 cell sheets through short-term osteogenic medium application. *Artif Cells, Nanomed Biotechnol* 2018;46(Suppl 2):1145—53.
27. Yang J, Zhang H, Chan SM, et al. TiO2 nanotubes alleviate diabetes-induced osteogenetic inhibition. *Int J Nanomed* 2020;15:3523—37.
28. Czekanska EM, Stoddart MJ, Ralphs JR, Richards RG, Hayes JS. A phenotypic comparison of osteoblast cell lines versus human primary osteoblasts for biomaterials testing. *J Biomed Mater Res* 2014;102:2636—43.
29. Ishikawa K, Abe S, Yawaka Y, Suzuki M, Watari F. Osteoblastic cellular responses to aluminosilicate nanotubes, imogolite using Saos-2 and MC3T3-E1 cells. *J Ceram Soc Jpn* 2010;118:516—20.
30. Peterson WJ, Tachiki KH, Yamaguchi DT. Serial passage of MC3T3-E1 cells down-regulates proliferation during osteogenesis in vitro. *Cell Prolif* 2004;37:325—36.
31. Xie Y, Chen X, Zheng X, et al. Beta1-integrin/Hedgehog-Gli1 signaling pathway fuels the diameter-dependent osteoblast differentiation on different TiO2 nanotubes: the optimal-diameter nanotubes for osteoblast differentiation. *Int J Biochem Cell Biol* 2021;137:106026.
32. Vimalraj S. Alkaline phosphatase: structure, expression and its function in bone mineralization. *Gene* 2020;754:144855.
33. Murray E, Provvedini D, Curran D, Catherwood B, Sussman H, Manolagas S. Characterization of a human osteoblastic osteosarcoma cell line (SAOS-2) with high bone alkaline phosphatase activity. *J Bone Miner Res* 1987;2:231—8.
34. Komori T. Regulation of proliferation, differentiation and functions of osteoblasts by Runx2. *Int J Mol Sci* 2019;20:1694.
35. Komori T. Whole aspect of Runx2 functions in skeletal development. *Int J Mol Sci* 2022;23:5776.
36. Brammer KS, Oh S, Cobb CJ, Bjursten LM, van der Heyde H, Jin S. Improved bone-forming functionality on diameter-controlled TiO(2) nanotube surface. *Acta Biomater* 2009;5:3215—23.
37. Brammer KS, Frandsen CJ, Jin S. TiO2 nanotubes for bone regeneration. *Trends Biotechnol* 2012;30:315—22.
38. Lv L, Liu Y, Zhang P, et al. The nanoscale geometry of TiO2 nanotubes influences the osteogenic differentiation of human adipose-derived stem cells by modulating H3K4 trimethylation. *Biomaterials* 2015;39:193—205.

39. Li Y, Wang S, Dong Y, et al. Effect of size and crystalline phase of TiO2 nanotubes on cell behaviors: a high throughput study using gradient TiO2 nanotubes. *Bioact Mater* 2020;5: 1062—70.

40. Filova E, Fojt J, Kryslova M, Moravec H, Joska L, Bacakova L. The diameter of nanotubes formed on Ti-6Al-4V alloy controls the adhesion and differentiation of Saos-2 cells. *Int J Nanomed* 2015;10:7145—63.